Synchronization and stimulated emission in an array of mechanical phase oscillators on a resonant support

David Mertens and Richard Weaver
Department of Physics, University of Illinois, Urbana, Illinois 61801, USA
(Received 23 December 2010; published 25 April 2011)

Inspired by recent laboratory observations, we propose a mechanical model for eccentrically weighted motors coupled through a vibrating plate. The equations are found to generalize those of Kuramoto to frequency- and position-dependent coupling. The behavior of the model, as determined analytically for no disorder and numerically for systems with and without quenched disorder, shows the key features observed in the laboratory, including hysteresis, bistability, and a spectral gap. The model exhibits stimulated emission and discontinuous lasinglike transitions.

DOI: 10.1103/PhysRevE.83.046221 PACS number(s): 05.45.Xt, 43.20.Tb, 42.55.Ah

I. INTRODUCTION

In recent years there has been considerable interest in dynamic synchronization in which sets of distinct coupled phase oscillators synchronize to each other. The phenomenon occurs in disparate circumstances, including firefly flashes [1], bridges with crowds of pedestrians [2], and chemical oscillations [3–5]. It occurs between lasers [6,7], thermoacoustic engines [8–10], Josephson junctions [11–13], metronomes [14], and pendulum clocks [15]. The chief mathematical model for studying the synchronization of large numbers of auto-oscillators is that of Kuramoto and its generalizations [3,16]. After arguing that the state of a limit-cycle oscillator is well represented in terms of its phase ξ and that the phase of each oscillator is weakly coupled to the phases of the others, Kuramoto [16] derived a set of N coupled Adler [17] equations:

$$\frac{d\xi_n}{dt} = \omega_n + \frac{1}{N}\sum_{m=1}^{N} A\ \sin(\xi_m - \xi_n). \tag{1}$$

Kuramoto showed that this model, in the limit $N \to \infty$, exhibits a second-order phase transition in which a macroscopic number of oscillators synchronize to each other if A is sufficiently large compared to the deviations among the many ω_n.

A more general model proposed by Winfree [18] predates Kuramoto's work. Kuramoto's model has the advantage that it admits exact solutions for its order parameter and other properties, providing a framework for generalizations. The Kuramoto model has been extended to include time delays [19], randomness in the couplings [20,21], and a spatial dependence of the couplings [21–23]. Recent monographs on synchronization include those of Pikovsky *et al.* [24] and Balanov *et al.* [25] and reviews of the Kuramoto model include those of Acebrón *et al.* [26] and Strogatz [27].

The synchronization transition in Josephson-junction arrays has been studied in the context of the Kuramoto model [13]. It has also been shown to have characteristics of a lasing transition [11]. Similar synchronization and laserlike behavior were observed in a system of piezoelectric auto-oscillators [28]. This raises the questions of what differentiates lasing from the synchronization exhibited in the Kuramoto model and how might the Kuramoto model be extended to obtain a lasing transition.

Lasing requires that the coupling be mediated by waves. In a laser, atomic oscillators are coupled by light waves. The piezoelectric auto-oscillators reported by Weaver *et al.* [28] were coupled through ultrasound. Josephson junctions can couple their oscillations through their mutual microwave radiation field [11]. In Ref. [29], for Huygen's clocks [15], for metronomes [14], and for the Millennium Bridge [2], coupling is through structural vibrations. Such systems will generally have couplings that depend on frequency and oscillator position. The coupling between oscillators in these systems may be neither uniform, as in the Kuramoto model, nor random, as in the model of Daido [20], but instead exhibit a complex spatial dependence related to the modes of the radiation field.

Systems with wave-mediated interactions often have frequency-dependent coupling. Yet synchronization among oscillators with frequency-dependent coupling is thus far poorly explored [30]. It is of interest in the field of synchronization for that reason, but also because such systems can readily be realized in the laboratory, their microphysics can be readily modeled and they are relevant to lasers.

The sine-qua-non of a laser is stimulated emission, in which a wave incident upon an oscillator is reemitted with unchanged phase and increased amplitude. Stimulated emission is a classical phenomenon [28,31–38] and is describable without quantum mechanics. A classical oscillator will exhibit stimulated emission or stimulated absorption, depending on the phase of its oscillation relative to that of an incident field. Thus an incoherent array of classical oscillators will show no net stimulated emission. If, however, all or most of the oscillators can be induced to have the same frequency and the correct phases, the set will exhibit stimulated emission. Only to the extent that oscillators and incident fields have the same frequency and the correct phase difference will the energy in the oscillators be transferred efficiently to the wave field and the net emitted wave be coherent. As described above, dynamic synchronization suggests that classical phase oscillators can be entrained to their mutual radiation field; they can synchronize to a common frequency with fixed phase differences. If these phase differences are such that each oscillator does work at a rate greater than it does without an incident field, i.e.,

if there is stimulated emission, the system will be a laser analog [11,28,31].

Classical laser designs have been proposed, but little has been realized in the laboratory. The designs of Borenstein and Lamb [31,32] and Kobelev *et al*. [34] are composed of incoherently excited Duffing oscillators. The oscillators emit spontaneously in a trivial fashion. Theoretical arguments indicate that, when they go into resonance with each other with the right phase relation as enforced by interactions with their mutual radiation field, they also emit by stimulated emission. An acoustic version has been realized by Bredikhin *et al*. [35], who present theory and measurements on a system of impulsively excited nonlinear bubbles. While ringing down, the bubbles sometimes synchronize by means of their nonlinearity and their mutual radiation field. Zavtrak and co-workers [36,37] suggested that bubbles or other particles in a fluid could be pumped by an applied coherent harmonic electric or acoustic field. They suggest that the particles would bunch spatially under the influence of radiation forces, leading to a coherent reemission of sound in a direction imposed by their radiation field and the modes of their cavity. This would be an acoustic version of a free-electron laser, or gyrotron [39].

We recently presented [29] a system of eccentrically weighted dc motors, the kind used as cell phone vibrators, mounted on a cantilevered plate. The laboratory system exhibited several intriguing behaviors, including synchronization, hysteresis, spectral gaps, and sudden changes in sound power output as a function of governing parameters. Here we intend to propose a model and theory for that and similar systems.

The laboratory system in Ref. [29] constitutes an additional acoustic analog for a laser, but is simpler than the bubbles of Zavtrak and co-workers [36,37] and Bredikhin *et al*. [35] and simpler than the piezoelectric limit-cycle auto-oscillators of Weaver and co-workers [28,38]. Furthermore, it is readily realized in the laboratory. The mechanical principles are straightforward: The eccentrically weighted dc motors apply vibrating forces to their support that depend on the speeds of the motors and on their first moments of inertia. These forces generate mechanical waves in the support. Conversely, motion of the support applies an effective torque on the motors that affects their speeds. Thus the motions of the motors and the support are coupled.

In Sec. II, governing equations similar to Eq. (1) are derived for the motors. Section III then presents analytic solutions of the model for the case of chief interest in which the support is dominated by isolated resonances and for the special analytically tractable case in which all motors have identical natural speeds. The analytic solutions show that an array of such motors on a resonant support can synchronize in a manner similar to, but more complex than, that of Kuramoto systems. Furthermore, such systems exhibit stimulated emission and superradiance, like lasers. Section IV presents numerical solutions for populations with and without disorder among the natural motor speeds and compares the results to the analytic solutions of Sec. III and to our previous laboratory observations.

II. MECHANICAL MODEL

Figure 1 shows one of the eccentrically weighted dc motors that we use in our laboratory [29] and describes an idealized mechanical model for the dynamics of the ith such motor in terms of its orientation $\theta_i(t)$ and the displacement $u_i(t)$ of the support under it. A force $f_i(t)$ acts upward on the motor and downward on the support. The rotor is taken to have moment of inertia I around its axis, first moment of mass λ, and total mass μ. The rest of the motor has mass m. A torque Γ is applied to the rotor by the motor, controlled by the current supplied to the motor. We neglect horizontal forces under the assumption that the support is stiff against horizontal motions. The motors are of the class called rotators and are simpler than limit-cycle oscillators [24,40]. The governing equations include torque balance,

$$I\frac{d^2\theta_i}{dt^2} = \Gamma_i - \alpha\frac{d\theta_i}{dt} + \lambda\sin\theta_i\frac{d^2u_i}{dt^2} \tag{2}$$

(where we have modeled the motor's drag with a viscous

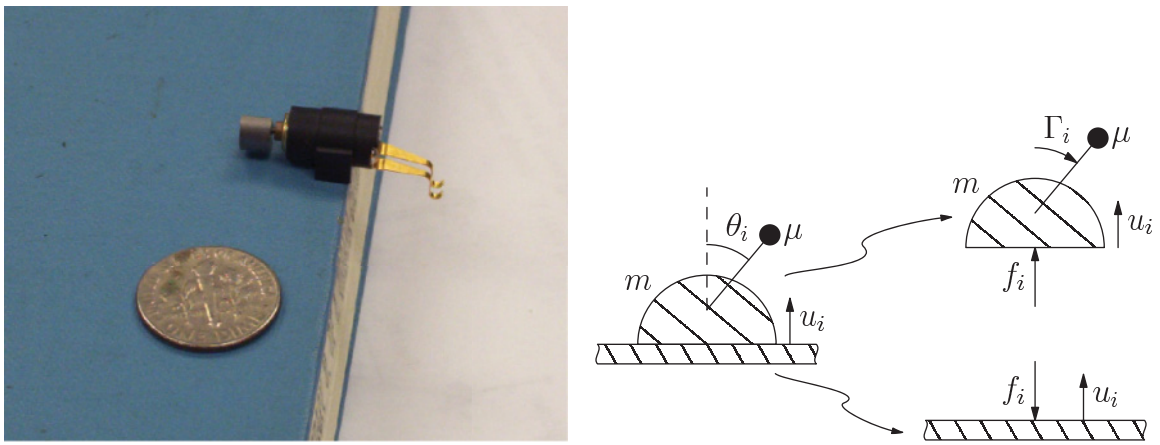

FIG. 1. (Color online) Photograph of a motor and an illustration. The mechanical model describes an eccentrically weighted dc motor on a compliant foundation. (The foundation, a thin aluminum plate, is not shown in the photograph.) The motor has total mass $m + \mu$. It has a rotor of mass μ, first moment of inertia λ, and second moment of inertia I. The rotor is subject to an applied torque Γ_i and a viscous drag (not illustrated).

coefficient α), and also force balance

$$f_i = (m+\mu)\frac{d^2u_i}{dt^2} + \lambda\frac{d^2\cos\theta_i}{dt^2}. \tag{3}$$

For linear systems such as the support, the displacements u_i at one location and time can be expressed as a convolution of a Green function with the forces f_j applied at other points and times. Using this formalism, we close the system of Eqs. (2) and (3) by writing

$$u_i = -\sum_j G_{ij} \otimes f_j, \tag{4}$$

where $\otimes$ represents a temporal convolution and G_{ij} is the Green function for the support. The minus sign arises from the oppositely defined direction for f and v. (Using this notation, we interpret Filatrella *et al.* [41] as closing their system of equations by relating u_i and f_j through a linear ordinary differential equation instead of a Green function.) Furthermore, we introduce an ancillary Green function g_{ij}, defined most readily in abstract terms and direct matrix notation:

$$\mathbf{g} = \left(\mathbf{G}^{-1} + (m+\mu)\mathbf{I}\frac{d^2}{dt^2}\right)^{-1}. \tag{5}$$

$\mathbf{g}$ may be interpreted as Green's function for the structure with added point masses $m+\mu$ at the positions of all the motors. Here $\mathbf{I}$ is the identity matrix. The present interest is in resonant supports, for which $\mathbf{g}$ will be best represented in its modal expansion, as summarized in the Appendix.

We use $\mathbf{g}$ to combine Eqs. (2) and (3) and eliminate the variables f and v, obtaining a set of integrodifferential equations for the θ:

$$I\frac{d^2\theta_i}{dt^2} = \Gamma_i - \alpha\frac{d\theta_i}{dt} + \lambda\sin\theta_i \times \sum_j \frac{d^2}{dt^2}\left[g_{i\,j} \otimes \left(-\lambda\frac{d^2\cos\theta_j}{dt^2}\right)\right]. \tag{6}$$

In the absence of coupling (e.g., $\lambda = 0$) each motor achieves a steady state at $\theta_i = \omega_i t + \theta_{i0}$ with a natural speed $\omega_i = \Gamma_i/\alpha$ and an arbitrary phase θ_{i0}. We imagine that weak coupling modifies this only slightly and so neglect the second time derivative on the left-hand side to simplify the governing equation:

$$\frac{d\theta_i}{dt} = \omega_i - \frac{\lambda^2}{\alpha}\sin\theta_i \sum_j \frac{d^2}{dt^2}\left[g_{ij} \otimes \left(\frac{d^2\cos\theta_j}{dt^2}\right)\right]. \tag{7}$$

It is for this integrodifferential equation that we will be seeking analytic and numeric solutions.

III. ANALYTIC SOLUTIONS

Without loss of generality we set $\theta_i(t) = \Omega t + \phi_i(t)$ with Ω to be determined:

$$\frac{d\phi_i}{dt} = \omega_i - \Omega - \frac{\lambda^2}{\alpha}\sin(\Omega t + \phi_i) \times \sum_j \frac{d^2}{dt^2}\left(g_{ij} \otimes \frac{d^2\cos(\Omega t + \phi_j)}{dt^2}\right). \tag{8}$$

We now apply a series of approximations to derive an expression that can be more easily interpreted. If the ϕ vary slowly, as they will if every motor has a speed at or close to Ω, then the effect of $\mathbf{g}$ can be approximated well in the frequency domain in terms of a transfer function $|\tilde{g}_{ij}(\Omega)|$ and a phase delay $\gamma_{ij}(\Omega)$, as in Eq. (A5). Similarly, each pair of time derivatives is well approximated by a factor of $-\Omega^2$:

$$\frac{d\phi_i}{dt} = \omega_i - \Omega - \frac{\lambda^2\Omega^4}{\alpha}\sin(\Omega t + \phi_i) \times \sum_j |\tilde{g}_{ij}(\Omega)|\cos[\Omega t + \phi_j - \gamma_{ij}(\Omega)]. \tag{9}$$

Using a trigonometric identity, we combine the sine and cosine terms on the right-hand side, leading to a rapidly varying part (at frequency 2Ω) and a slowly varying part. We eliminate the rapidly varying part by averaging over one cycle, giving

$$\frac{d\phi_i}{dt} = \omega_i - \Omega - \frac{\lambda^2\Omega^4}{2\alpha} \times \sum_j |\tilde{g}_{ij}(\Omega)|\sin[\phi_i - \phi_j + \gamma_{ij}(\Omega)]. \tag{10}$$

Each of the diagonal elements of the Green's function of a dissipative structure must have a positive imaginary part [42], i.e., $\sin\gamma_{ii} \geqslant 0$, so we restrict our attention to $0 \leqslant \gamma_{ii} \leqslant \pi$.

The Kuramoto equations are recovered if the i, j, and Ω dependence in $\mathbf{g}$ is neglected and if the γ_{ij} are zero. Sakaguchi and Kuramoto [43] have considered the effect of a constant, uniform phase delay $\gamma_{ij} \equiv \gamma$. To our knowledge, no one has examined Ω dependence. In the case of a highly resonant support, $\eta \ll 1$, Ω dependence can be strong.

Synchronization in the above system is complex. The parameter space is large. Simplification and insight can be obtained by analyzing special cases. One is to allow all motors to be identical, $\omega_i = \omega$ for all i. Furthermore, we require all motors to be coupled identically, independently of i and j, a condition that applies to the experiments [29] but not generally. Thus $g_{ij}(\Omega) = g(\Omega)$, $\gamma_{ij}(\Omega) = \gamma(\Omega)$, and we have

$$\frac{d\phi_i}{dt} = \omega - \Omega - \frac{\lambda^2\Omega^4}{2\alpha}\sum_j |g(\Omega)|\sin[\phi_i - \phi_j + \gamma(\Omega)]. \tag{11}$$

The synchronized state is now easy to identify: It corresponds to $\phi_i = 0$ for all i and requires

$$\Omega = \omega - \frac{N\lambda^2\Omega^4}{2\alpha}|\tilde{g}|\sin\gamma = \omega - \frac{N\lambda^2\Omega^4}{2\alpha}\mathrm{Im}[\tilde{g}(\Omega)]. \tag{12}$$

The state is such that all motors have identical phases and run at speed Ω diminished from their natural speed ω by an amount that scales with N and with the positive quantity $|g|\sin\gamma$. One can further show that the acoustic power output of the N motors is the difference between the rate of work done by the torques Γ and the loss in the viscous mechanisms, i.e.,

$$N(\Gamma\Omega - \alpha\Omega^2) = N\Omega\alpha(\omega - \Omega) \tag{13}$$

$$= \tfrac{1}{2}N^2\lambda^2\Omega^5|g|\sin\gamma. \tag{14}$$

Inasmuch as this scales with the square of the number of motors, the system is exhibiting stimulated emission and super radiance. By linearizing Eq. (11) around the synchronized state $\phi_i = 0$ for all i, it is not hard to show that the synchronized state is stable against all infinitesimal perturbations (except the trivial marginally stable perturbation of a uniform shift of all ϕ) if and only if the real part of the Green's function is positive, i.e., $\cos\gamma > 0$.

Another solution to Eq. (11) is apparent, in which the θ are distributed uniformly between 0 and 2π:

$$\theta_i = \omega t + \frac{2\pi i}{N}, \tag{15}$$

for a suitable ordering of the θ_i. This state has $N-2$ neutrally stable linear perturbations. The two remaining perturbations exhibit time dependence proportional to $e^{\nu t}$ with

$$\nu = N\frac{\lambda^2\omega^4}{4\alpha}e^{\pm\imath\gamma}|\tilde{g}(\gamma)|. \tag{16}$$

On the stiffness-controlled low-frequency side of a resonance, where $0 < \gamma < \pi$, these dispersed states are unstable. On the mass-controlled high-frequency side of a resonance, the Green function has a negative real part (i.e., $\frac{\pi}{2} < \gamma < \pi$), making the modes exponentially stable.

Figure 2 plots the solution $\Omega(\omega)$ to Eq. (12) for the case of a single resonance [the sum over r in Eq. (A2) has one term]. We plot

$$\Omega = \omega - \frac{M_r X\Omega^4}{2}\mathrm{Im}[\tilde{g}^r(\Omega)] \tag{17}$$

$$= \omega - X\frac{\eta_r\omega_r\Omega^5}{(2\eta_r\omega_r\Omega)^2 + \left(\omega_r^2 - \Omega^2 + \eta_r^2\omega_r^2\right)^2}, \tag{18}$$

where we have introduced a coupling strength parameter $X = N\lambda^2/\alpha M_r$. The coupling strength is measured in units of seconds per radian. The loss tangent η is defined in the Appendix.

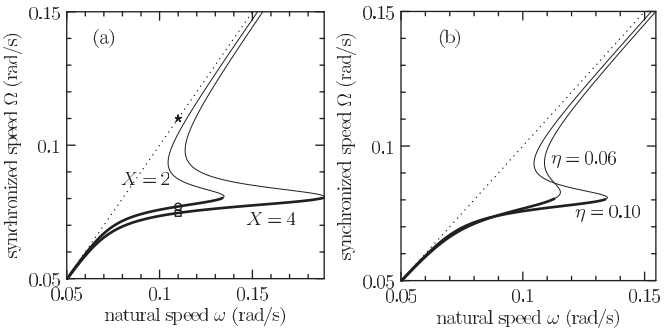

FIG. 2. Representative cases for Ω, the speed of the synchronized state, as a function of the natural speeds ω of the motors, according to Eq. (18). The bold lines are the solutions that we expect to be stable because the imaginary part of $\tilde{\mathbf{g}}$ is positive. The thin lines are solutions for which the imaginary part of $\tilde{\mathbf{g}}$ is negative and should be unobservable in practice. The dotted line $\Omega = \omega$ is provided for reference. For all four curves, the resonant frequency ω_r is 0.08 rad/s. (a) Curves for two different couplings X and the same loss tangent η of 0.06. (b) Curves for two different loss tangents η but identical coupling $X = 2$ s/rad. The star, circle, and square in (a) are related to Figs. 4 and 5 and are discussed in Sec. IV A.

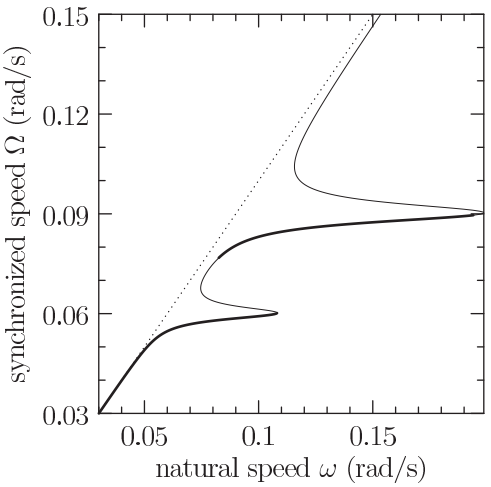

FIG. 3. Solution to Eq. (12) for the case in which the Green function $\mathbf{g}$ has two resonances. For the meaning of the line weights, see Fig. 2. The resonances have identical coupling strengths X_1 and X_2 of 2.0 s/rad and identical loss tangents η_1 and η_2 of 0.038, but different resonant frequencies $\omega_1 = 0.06$ rad/s and $\omega_2 = 0.09$ rad/s.

For a single resonance, the stability criterion $\cos\gamma > 0$ is satisfied only for $\Omega < \omega_r\sqrt{1+\eta_r^2}$. Thus, by this theory one expects to see no synchronization at speeds Ω on the mass-controlled high-frequency side of a resonance, regardless of the driving torques and the natural motor speeds ω. Solutions to Eq. (18) that fail this criterion are distinguished in the figure from those that satisfy it. The nearly flat regions for the synchronized speed Ω in the vicinity of 0.075 rad/s correspond to the speed of the synchronized state being almost independent of torque. For very high driving torque, however, the synchronized state loses its stability.

A plot for the more complex case of two resonances is given in Fig. 3. Each resonance gives rise to a range of natural speeds ω for which the synchronization speed Ω is slightly less than a resonance frequency and nearly independent of the natural speed. These ranges overlap for the two resonances, leading to a regime—ω between 0.08 and 0.11 rad/s—in which the system can synchronize at either of two speeds Ω. Furthermore, there is a range of Ω from 0.06 to 0.075 rad/s in which the system cannot oscillate. All of these echo observations are reported in Ref. [29] and arise in our numerics in the following section, even those involving disorder.

IV. NUMERICAL SOLUTIONS

Practical systems, such as that discussed in Ref. [29], are disordered in the sense that natural motor speeds vary among the motors. Such a generalization does not readily lend itself to the analysis of Sec. III. Nor does the preceding analysis shed much light on the dynamics: How does the system approach the stable synchronized state? Nor does it shed light on errors that may have been introduced by the short time averaging used to eliminate the terms in 2Ω. For all those reasons, we now turn to numerical solutions.

Numerical solutions of Eq. (7) were examined for their correspondence to the simple model discussed in Sec. III and

our previous laboratory observations [29]. We rewrite Eq. (7) using a modal expansion for the Green function:

$$\frac{d\theta_i}{dt} = \omega_i - \frac{1}{N}\sin\theta_i \sum_{r,j} \frac{d^2}{dt^2}\left(X_r h^r \otimes \frac{d^2\cos\theta_j}{dt^2}\right), \quad (19)$$

where we take the ancillary Green function for each resonance h^r in the form

$$h^r(\tau) = \sin(\omega_r\tau)\frac{e^{-\eta\omega_r\tau}}{\omega_r}. \quad (20)$$

The resonances are labeled by r and factors of λ^2, α, and M have been absorbed into the coupling strengths X_r, as in Sec. III.

Numerical solutions of Eq. (19) are of necessity approximate. We employ a simple Euler tangent approximation for the first time derivative and evaluate the convolution by discrete integrations and the second time derivatives by discrete differencing. We define our units such that a single time step is 1 s. We choose motor speeds of about 0.1 rad/s, meaning the motors advance their phases by about 0.1 rad each time step. The scheme is prohibitively implicit if these second derivatives are evaluated centrally; they are therefore evaluated with a delay of one time step. While the resulting time series will differ from exact solutions of the original equations, we expect the qualitative behavior to be correct. All studies are for $N = 100$.

In Sec. III, Ω was used to refer to the speed at which the motors synchronized. Since that population of motors had no disorder, the synchronized speed was identical to the average speed. We will consider populations with disorder in this section and we will redefine Ω as the average motor speed:

$$\Omega = \frac{1}{N}\sum_i \dot\theta_i. \quad (21)$$

A. Approach to the steady state

We first evaluate how the system evolves from random initial conditions. A qualitative steady state is typically achieved after times of the order of 2000 s. Figures 4–6 show the evolution of the speeds (averaged over 16 time steps) of 11 arbitrarily chosen motors. They also show the evolution of an order parameter defined as

$$R = \frac{1}{N}\left|\sum_i e^{\iota\theta_i}\right|. \quad (22)$$

This order parameter, taken directly from Kuramoto's treatment, can be thought of as a vector sum of the motor phases. If the motors are in phase, R will be close to 1; if they are uniformly distributed between 0 and 2π, R will be close to 0; and if the motors have random phases, R will exhibit random fluctuations about a rms of $N^{-1/2} = 0.1$. The resonant frequency ω_r is the same among all three figures (0.08 rad/s) and the loss tangent η is the same (0.06). The figures differ only in their coupling strengths X and the presence or absence of quenched disorder among the motors' natural speeds.

In the simulation shown in Fig. 4, the motors settle at their natural speed of 0.11 rad/s. According to Eq. (18) (and indicated by the open circle in Fig. 2), there is a synchronized

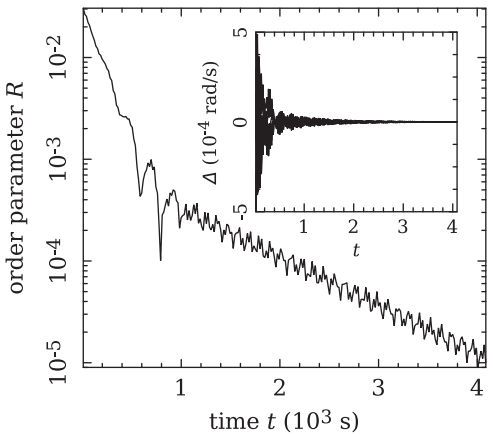

FIG. 4. Order parameter R and discrepancy $\Delta_i \equiv \dot\theta_i - \omega$ between instantaneous motor speeds and the natural motor speed for 100 identical motors. The initial phases are distributed randomly. For these plots, the natural speed of the motors ω is 0.11 rad/s. There is a single resonance with frequency ω_r of 0.08 rad/s, a loss tangent η of 0.06, and a coupling strength X of 2 s/rad. The inset shows how the instantaneous speeds differ from the natural speed of 0.11 rad/s for 11 arbitrarily chosen motors. The final state corresponds to the star in Fig. 2(a).

speed Ω of 0.075 rad/s. The motors do not choose that solution, even when slight noise is artificially introduced. The motors settle instead into a state, indicated in Fig. 2 by a star, in which each motor is going at close to its natural speed. The order parameter decreases exponentially, which agrees with the prediction in Sec. III of exponential stability of the uniformly distributed state. In other simulations, with different initial conditions, we were able to obtain synchronized behavior with mean speed Ω that matched the prediction of 0.075 rad/s. Thus both the synchronized and the uniformly distributed states are stable, as predicted.

At a greater coupling strength of $X = 4$ s/rad, as in Fig. 5, the behavior is very different. After a transient, the motors synchronize at a speed of $\Omega = 0.073$ rad/s and an order

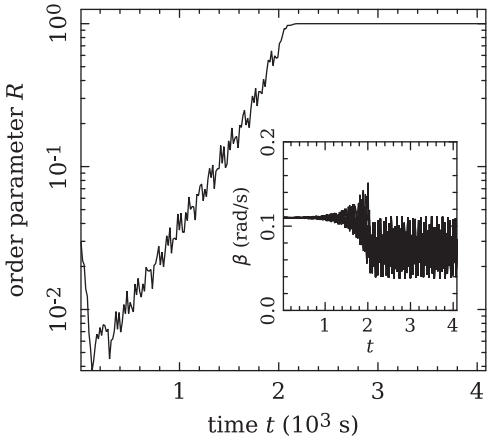

FIG. 5. Order parameter R and representative speeds $\beta_i \equiv \dot\theta_i$ for a simulation of 100 identical motors with initial phases distributed randomly. In contrast to Fig. 4, the coupling strength X of the resonance is 4 s/rad; all other parameters are identical. The final state corresponds to the open square in Fig. 2(a).

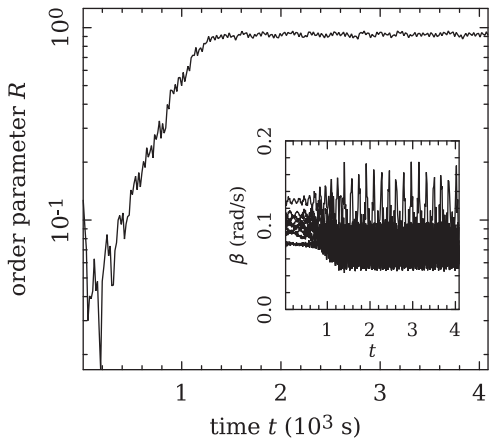

FIG. 6. Order parameter R and representative motor speeds $\beta_i \equiv \dot{\theta}_i$ for a disordered population of 100 motors, started from initially random phases. The resonance parameters are the same as in Fig. 4, except the coupling X is 2.9 rad/s. The natural frequencies are chosen from a Gaussian distribution with mean $\bar{\omega}$ of 0.1 rad/s and standard deviation σ of 0.01 rad/s (i.e., 10% of $\bar{\omega}$).

parameter of unity. The late time behavior shows a residual oscillation at a rate 2Ω, neglected in deriving Eq. (12). The open box in Fig. 2 is the corresponding prediction, a speed of $\Omega = 0.0745$ rad/s. The discrepancy may be due to numerical imprecision in computing Ω from the data in Fig. 5; it may be because the neglected oscillations at speed 2Ω are indeed significant; it may be due to the discretization in the implementation of the numerics. Whatever the source of the discrepancy, it is small and the decision to neglect fluctuations of frequency 2Ω in deriving Eq. (11) appears justified.

Figure 6 shows a case of disorder in the distribution of motor speeds. By introducing a Gaussian distribution of natural motor speeds with a standard deviation of 10% (i.e., $\bar{\omega} = 0.1$ rad/s and $\sigma = 0.01$ rad/s), we find that a few of the motors have left the pack and the order parameter is reduced below unity. Like the motor behavior presented in Figs. 4 and 5, the motors in Fig. 6 approach their steady-state behavior exponentially and in about 15 cycles. These compare favorably with observations from the laboratory [29], in which transient behavior was so fast that it was not measurable.

B. Numerical solutions for swept natural motor speeds

In the laboratory [29], behavior was monitored as a function of driving voltage, which determines torques and thus serves as a proxy for mean natural motor speed. The voltage was slowly swept, in a stepwise fashion, from a low to a high or a high to a low value, giving the motors time to adjust at each value. The laboratory system had two resonances and was noteworthy for a parameter regime in which the system could synchronize at either of two distinct frequencies, a behavior termed birythmic [44]. Each such frequency was slightly below one of the plate's resonant frequencies. Which frequency the system chose was a function of its history. It was also noteworthy for its observation of a spectral gap, a frequency range between the resonant frequencies in which the system was never seen to oscillate coherently. As discussed above, these features were exhibited in the analytic solutions of Fig. 3.

Birythmic hysteresis and a spectral gap are behaviors seen in the numerics also. Numerical simulations were conducted for the integrodifferential equations

$$\frac{d\theta_i}{dt} = \omega_i - \frac{1}{N}\sin\theta_i \sum_j \frac{d^2}{dt^2}\left(h \otimes \frac{d^2\cos\theta_j}{dt^2}\right), \qquad (23)$$

again with Green's function independent of i and j, but now corresponding to a set of motors on a support with two resonances:

$$h(\tau) = X_1 \sin(\omega_{r1}\tau)\frac{e^{-\eta_1\omega_{r1}\tau}}{\omega_{r1}} + X_2 \sin(\omega_{r2}\tau)\frac{e^{-\eta_2\omega_{r2}\tau}}{\omega_{r2}}. \qquad (24)$$

Analytic predictions for this two-resonance structure are shown in Fig. 3.

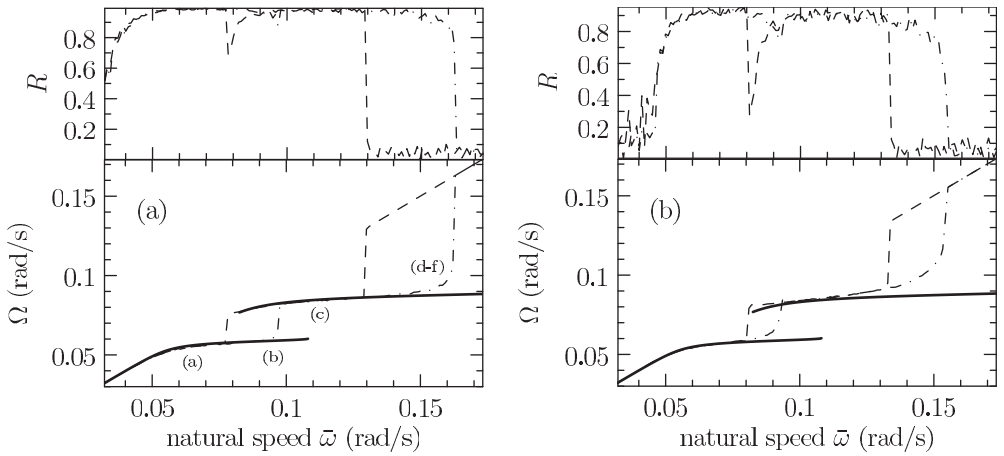

FIG. 7. Order parameter R and average motor speeds Ω for sweeps of mean natural motor speed $\bar{\omega}$ from 0.03 to 0.2 rad/s (dash-dotted curves) and then back to 0.03 rad/s (dashed curves), for disordered populations. In (a) the standard deviation of the natural motor speeds ω_i is $\sigma = 0.05\bar{\omega}$, whereas in (b) it is $\sigma = 0.1\bar{\omega}$. These results correspond to $X_1 = X_2 = 2.0$ s/rad, $\omega_{1r} = 0.06$ rad/s, $\omega_{2r} = 0.09$ rad/s, and $\eta_1 = \eta_2 = 0.038$. The solid curves indicate stable solutions for no disorder from Eq. (12) and plotted in Fig. 3. The marked locations in (a) correspond to the spectral power densities of Fig. 8.

The numerical simulations were performed in sweeps of 256 blocks. Mimicking the laboratory measurements, each block had three phases of 1024 s apiece: a sweep phase, a hold phase, and a measure phase. During the sweep phase, the natural speeds were slowly increased or decreased at a rate of $2^{-20} = 9.54 \times 10^{-7}$ rad/s^2. During the hold phase, the natural speeds were held fixed to allow transients to dissipate [45]. As such, the total number of time steps for a single upward or downward sweep was $256 \times 3 \times 1024$. During the measure phase, the natural speeds were again held fixed and we measured time series for the instantaneous speeds $\dot{\theta}_i$, order parameter R, and other data.

Cases were run in which every motor had identical natural motor speed ω_i and the results corresponded very closely to the predictions of Sec. III, in particular to the curves of Fig. 3. Figure 7 shows the mean motor speed Ω as a function of mean natural motor speed $\bar{\omega}$, for the case of disorder. For reference, we have included the stable solutions of Fig. 3. Natural motor speeds were taken randomly from a Gaussian distribution with a nonzero mean $\bar{\omega}$ and with a width of 5% or 10% of the mean for Figs. 7(a) and 7(b), respectively. We maintained the percentage width of the population throughout the simulations by stretching or compressing the population as we increased or decreased the mean natural motor speed $\bar{\omega}$.

The numerical and theoretical results plotted together in Fig. 7 agree nicely. The sweep of the solution of the coupled ordinary differential equations [Eq. (19)] reproduces much of the behavior predicted by the simpler analytic model of Eq. (12) and found also in the laboratory measurements (Fig. 7 of Ref. [29]). We note in particular the birythmic hysteresis, the spectral gap, and the wide regions in $\bar{\omega}$ over which Ω is nearly constant at a value a bit less than ω_r. (The upper hysteresis loop, which pertains to just one resonance, is likely similar to that reported by Filatrella *et al.* [41], who swept coupling strength X, not $\bar{\omega}$.) Neither disorder nor modeling of the fast time scales (ignored in Sec. III) have qualitatively changed these features.

Disorder has displaced and reduced some of the sharp features in $\Omega(\bar{\omega})$. Transitions in the order parameter remain sharp, suggesting that mean speed Ω fails to fully represent the state of the system. For that purpose, it may be better to address the chief interest for lasers: the spectral density of the wave power radiated by the oscillators.

C. Spectral power density and lasing transition

The energy radiated into the support by the motors can be written as a time integral of force times velocity. The work done is

$$W = -\int \sum_i f_i(t) \frac{d}{dt} v_i(t)\, dt. \tag{25}$$

By expressing the displacements v_i in terms of the forcing f_i and the Green function $\mathbf{G}$ and using Parseval's identity, we can rewrite the preceding equation as

$$W = \frac{-1}{2\pi} \int \imath\omega \sum_{i,j} \tilde{f}_i^*(\omega) \tilde{G}_{ij}(\omega) \tilde{f}_j(\omega)\, d\omega \tag{26}$$

$$= \frac{-1}{2\pi} \int \imath\omega \sum_{i,j} \tilde{q}_i^*(\omega) \tilde{g}_{ij}(\omega) \tilde{q}_j(\omega)\, d\omega, \tag{27}$$

where

$$q_i(t) = f_i(t) - (m+\mu)\ddot{v}_i \tag{28}$$

$$= \lambda \frac{d^2}{dt^2} \cos\theta_i. \tag{29}$$

This permits us to identify a spectral power density:

$$\Pi(\omega) = \frac{-1}{\pi} \mathrm{Im}\left(\sum_{i,j} \omega \tilde{q}_i^*(\omega) \tilde{g}_{ij}(\omega) \tilde{q}_j(\omega) \right). \tag{30}$$

The spectral power density can be evaluated as a function of frequency by a short-time Fourier transform over data from the numerical solutions, as in Fig. 8. In that figure, the frequency resolution $\Delta\omega$ is $2\pi/4096$ rad/s, corresponding to time records with 4096 samples.

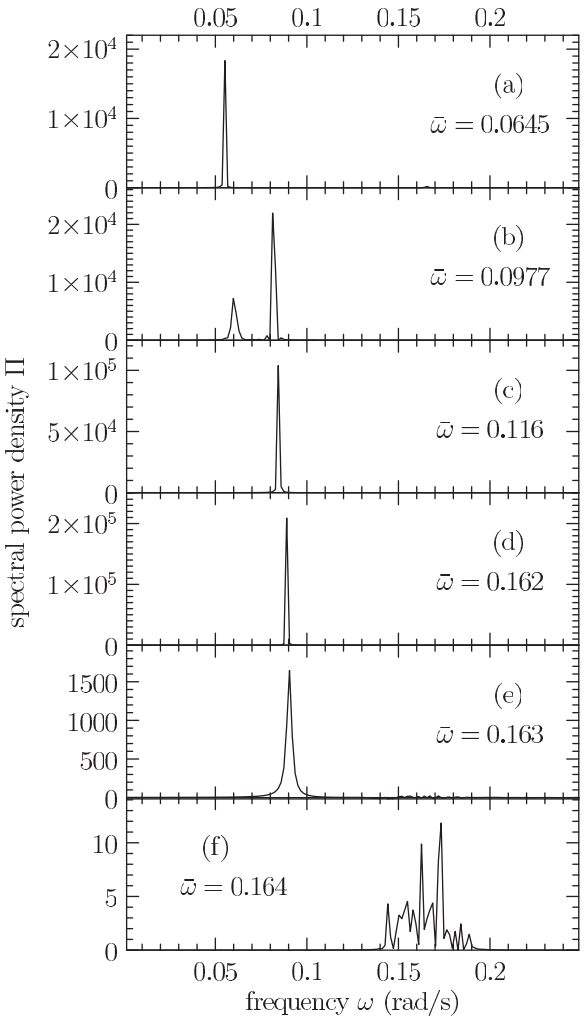

FIG. 8. Spectral power density vs frequency. The data for these figures are from the same upward run as the data in Fig. 7(a) and correspond to the labels in that figure. The means of the natural speeds are indicated. Note that the differences in natural speeds among (d)–(f) are small—the transition is abrupt.

Figures 8(a)–8(f) correspond to the labels in Fig. 7(a). Figures 8(a)–8(e) show that the power output is strong and confined to one or two narrow peaks. The width of the peaks appears to be governed by the resolution of the discrete Fourier transform. Figure 8(b) is of particular interest since it indicates lasing in two modes simultaneously, like a multimode laser. In Fig. 8(f), the power output is weak, broadband, and noisy. The small differences in mean natural motor speed across Figs. 8(d)–8(f) show that transitions between the various states can be abrupt. This corresponds to the sudden changes in audible power output observed in Ref. [29] and is reminiscent of a lasing transition.

The frequency at which $\Pi(\omega)$ peaks, as shown in Fig. 8, is not always the same as the average motor speed Ω shown in Fig. 7. Consider the cases in Figs. 8(d) and 8(e), for which $\bar{\omega} = 0.162$ and 0.163 rad/s. The dash-dotted line in Fig. 7 indicates a measured average motor speed Ω of about 0.095 rad/s, whereas the power output in Figs. 8(d) and 8(e) show peaks just below the resonant frequency, 0.09 rad/s. The peak of the power output is biased toward the motors operating near a resonance, making the frequency of the maximum power output distinct from the average motor speed [46].

V. CONCLUSION

The mechanical model introduced in Sec. II has been found to reproduce behaviors observed in the laboratory [29]. Its analytic and numerical solutions replicate those experimental observations, in particular by exhibiting hysteresis, the spectral gap, the broad regime in which Ω is independent of driving torque, and sharp transitions. The solutions also confirm the surmise that this system forms an acoustic analog to a laser. They show stimulated emission, super radiance, and sharp lasinglike transitions between a parameter regime in which spectral power radiation is wideband, noisy, and weak and one in which it is strong and dominated by narrow emission lines.

ACKNOWLEDGMENT

This work was supported by a grant of computational resources, on a SGI Altix, from the National Center for Supercomputing Applications.

APPENDIX : MODAL REPRESENTATION FOR THE GREEN'S FUNCTION

It is often convenient to represent $\mathbf{g}(t)$ and its Fourier transform $\tilde{\mathbf{g}}(\omega)$ as a sum over natural modes r:

$$g_{ij}(t) = \sum_r g^r(t) u_i^r u_j^r, \tag{A1}$$

$$\tilde{g}_{ij}(\omega) = \sum_r \tilde{g}^r(\omega) u_i^r u_j^r. \tag{A2}$$

Each resonance has a frequency ω_r, modal mass M_r, and decay time T_r. Here u_i^r is the rth resonance's displacement amplitude [not $u_i(t)$] at the position of the ith motor. We relate the decay times to the resonant frequencies by the (unitless) loss tangent $\eta_r \equiv (\omega_r T_r)^{-1}$, allowing us to express the Green function from a single resonance as

$$g^r(t) = \sin(\omega_r t) \frac{e^{-\eta_r \omega_r t}}{M_r \omega_r}, \tag{A3}$$

$$\tilde{g}^r(\omega) = \int_0^\infty g_{ij}(t) e^{\imath \omega t} dt = \frac{M_r^{-1}}{(\eta_r \omega_r - \imath \omega)^2 + \omega_r^2}. \tag{A4}$$

$\tilde{g}^r$ represents the Fourier transform of the resonance and $\imath = \sqrt{-1}$. We will also sometimes make use of the magnitude and phase of the Fourier transform of the Green function or its resonances:

$$\tilde{g}_{ij}(\omega) \equiv |\tilde{g}_{ij}(\omega)| e^{\imath \gamma_{ij}(\omega)}, \tag{A5}$$

$$\tilde{g}_{ij}^r(\omega) \equiv |\tilde{g}_{ij}^r(\omega)| e^{\imath \gamma_{ij}^r(\omega)}. \tag{A6}$$

[1] J. B. Buck, Q. Rev. Biol. **13**, 301 (1938).
[2] S. Strogatz, D. Abrams, A. McRobie, B. Eckhardt, and E. Ott, Nature (London) **438**, 43 (2005).
[3] Y. Kuramoto, *Chemical Oscillations, Waves, and Turbulence* (Springer-Verlag, New York, 1984).
[4] I. Z. Kiss, Y. Zhai, and J. L. Hudson, Science **296**, 1676 (2002).
[5] I. Z. Kiss, Y. Zhai, and J. L. Hudson, Phys. Rev. E **77**, 046204 (2008).
[6] S. Yu. Kourtchatov, V. V. Likhanskii, A. P. Napartovich, F. T. Arecchi, and A. Lapucci, Phys. Rev. A **52**, 4089 (1995).
[7] K. Y. Tsang, R. E. Mirollo, S. H. Strogatz, and K. Wiesenfeld, Physica D **48**, 102 (1991).
[8] G. W. Swift, J. Acoust. Soc. Am. **84**, 1145 (1988).
[9] P. S. Spoor and G. W. Swift, J. Acoust. Soc. Am. **106**, 1353 (1999).
[10] P. S. Spoor and G. W. Swift, J. Acoust. Soc. Am. **108**, 588 (2000).
[11] P. Barbara, A. B. Cawthorne, S. V. Shitov, and C. J. Lobb, Phys. Rev. Lett. **82**, 1963 (1999).
[12] P. Hadley, M. R. Beasley, and K. Wiesenfeld, Phys. Rev. B **38**, 8712 (1988).
[13] K. Wiesenfeld, P. Colet, and S. H. Strogatz, Phys. Rev. Lett. **76**, 404 (1996).
[14] J. Pantaleone, Am. J. Phys. **70**, 992 (2002).
[15] B. Bennett, M. F. Schatz, H. Rockwood, and K. Wiesenfeld, Proc. R. Soc. London Ser. A **458**, 563 (2002).
[16] Y. Kuramoto, in *Self-Entrainment of a Population of Coupled Nonlinear Oscillators*, edited by H. Aroki, Lecture Notes in Physics Vol. 39 (Springer-Verlag, Berlin, 1975), p. 420.
[17] R. Adler, Proc. IRE **34**, 351 (1946).
[18] A. T. Winfree, J. Theor. Biol. **16**, 15 (1967).

[19] M. K. S. Yeung and S. H. Strogatz, Phys. Rev. Lett. **82**, 648 (1999).
[20] H. Daido, Phys. Rev. Lett. **68**, 1073 (1992).
[21] T. E. Lee, G. Rafael, M. C. Cross, O. Kogan, and J. L. Rogers, Phys. Rev. E **80**, 046210 (2009).
[22] Y. Kuramoto and D. Battogtokh, Nonlinear Phenom. Complex Syst. **5**, 380 (2002).
[23] D. M. Abrams and S. H. Strogatz, Int. J. Bifurcation Chaos **16**, 21 (2006).
[24] A. Pikovsky, M. Rosenblum, and J. Kurths, *Synchronization: A Universal Concept in Nonlinear Sciences* (Cambridge University Press, Cambridge, 2001).
[25] A. Balanov, N. Janson, D. Postnov, and O. Sosnovtseva, in *Synchronization: From Simple to Complex*, Springer Series in Synergetics Vol. XIV (Springer-Verlag, Berlin, 2009), p. 237.
[26] J. A. Acebrón, L. L. Bonilla, C. J. Pérez Vicente, F. Ritort, and R. Spigler, Rev. Mod. Phys. **77**, 137 (2005).
[27] S. H. Strogatz, Physica D **143**, 1 (2000).
[28] R. Weaver, O. Lobkis, and A. Yamilov, J. Acoust. Soc. Am. **122**, 3409 (2007).
[29] D. Mertens and R. Weaver, Complexity, doi: 10.1002/cplx.20352.
[30] Frequency-dependent coupling is implicit, though not so termed, in the Millennium Bridge [2], in Josephson-junction arrays coupled through a mutual load [41], and in systems with time delays [19].
[31] M. Borenstein and W. E. Lamb, Phys. Rev. A **5**, 1298 (1972).
[32] M. Sargeant III, M. O. Scully, and W. E. Lamb, Jr., *Laser Physics* (Addison-Wesley, Reading, MA, 1974).
[33] B. Fain and P. W. Milonni, J. Opt. Soc. Am. B **4**, 78 (1987).
[34] Y. A. Kobelev, L. A. Ostrovsky, and I. A. Soustova, Zh. Eksp. Teor. Fiz. **99**, 470 (1991) [Sov. Phys. JETP, **72**, 262 (1991)].
[35] V. V. Bredikhin, Yu. A. Kobelev, and N. I. Vasilinenko, J. Acoust. Soc. Am. **103**, 1775 (1998).
[36] S. T. Zavtrak, J. Acoust. Soc. Am. **99**, 730 (1996).
[37] I. V. Volkov, S. T. Zavtrak, and I. S. Kuten, Phys. Rev. E **56**, 1097 (1997).
[38] A. Yamilov, R. Weaver, and O. Lobkis, Photonics Spectra **40**, 90 (2006).
[39] B. G. Danly and R. J. Temkin, Phys. Fluids **29**, 561 (1986).
[40] I. I. Blekhman, P. S. Landa, and M. G. Rosenblum, Appl. Mech. Rev. **48**, 733 (1995).
[41] G. Filatrella, N. F. Pedersen, and K. Wiesenfeld, Phys. Rev. E **75**, 017201 (2007).
[42] Supports of physical interest lose energy to heat and acoustic radiation. This energy must come from the motors, which requires that velocity responses be in phase with the forcing.
[43] H. Sakaguchi and Y. Kuramoto, Prog. Theor. Phys. **76**, 576 (1986).
[44] V. Casagrande and A. S. Mikhailov, Physica D **205**, 154 (2005).
[45] The hold phase is only 1024 s, which is shorter than the reported transient times in Sec. IV A. However, those transient times are for a system starting from completely random initial conditions; the motors in the sweeps are not so disordered and do not need as much time for their transient to diminish.
[46] Depending on the experimental setup, it may be possible to correct for this bias and extract, from the spectral power output, the number of motors operating at each frequency. We described one such technique in Ref. [29].